





RESEARCH ARTICLE

10.1029/2021GC009923

Raman Spectral Shifts in Naturally Faulted Rocks

D. K. Muirhead¹ , L. Kedar¹, A. Schito^{1,2} , S. Corrado² , C. E. Bond¹ , and C. Romano²

¹Department of Geology and Petroleum Geology, School of Geosciences, University of Aberdeen, Aberdeen, UK,

²Dipartimento di Scienze, Sezione di Scienze Geologiche, Università degli Studi Roma Tre, Roma, Italy

Key Points:

- Raman spectroscopy applied to faulted and non-faulted rocks to assess the nature of peak shift in relation to faulted context
- A shift in Raman parameters between faulted and non-faulted samples is exhibited; however, the direction and magnitude of this shift varies
- Systematic sampling is needed across fault zone study areas to allow for detailed structural analyses

Correspondence to:

D. K. Muirhead,
dmuirhead@abdn.ac.uk

Citation:

Muirhead, D. K., Kedar, L., Schito, A., Corrado, S., Bond, C. E., & Romano, C. (2021). Raman spectral shifts in naturally faulted rocks. *Geochemistry, Geophysics, Geosystems*, 22, e2021GC009923. <https://doi.org/10.1029/2021GC009923>

Received 20 MAY 2021

Accepted 4 OCT 2021

Abstract Raman spectral shifts of carbonaceous materials arising from faulted rocks produce varied and complex results. By analyzing faulted and adjacent non-faulted samples from three discrete localities in France, Italy, and Morocco, we assess changes in specific Raman parameters, including G-peak width, G-peak position, and peak intensity ratios. We consistently observe a shift in Raman parameters between faulted and non-faulted samples; however, the direction and magnitude of this shift varies. Raman peak intensity ratios are shown to both increase and decrease on fault planes. The majority of samples exhibit decreasing peak width and peak position in the faulted samples, but this is not consistent; in two samples an increase is observed, but the shift tends to be small. These data are compared to published Raman spectral shifts from experimental fault data. Our results suggest that fault zone deformation processes may measurably change the carbon nanostructure in faulted rocks. The inconsistent nature of Raman spectral shifts in the fault rock samples analyzed, and those published suggest that a complex set of factors control carbon nanostructure changes in fault rocks. These factors, although not discriminated here, likely include, background temperature, frictional heating, strain, carbonaceous material type, amongst others. We have shown that Raman Spectral shifts occur in faulted rocks with implications for how Raman data are used to predict maximum temperatures in faulted sedimentary rocks. We recognize the potential for a range of fault zone processes to modify Raman spectral shifts, however, systematic sampling across individual fault zones is critical.

Plain Language Summary Faulting in rocks (which can cause earthquakes) can create structural changes to materials at the fault surface. Here we have investigated the effects of faulting on carbon in various localities from France, Italy and Morocco. Carbon can be analyzed using a technique called Raman spectroscopy, which can attribute a structural order to the material, in a sense telling us how altered it has become at the fault surface. We present data that show the complexity of faulted systems, with structural changes to carbon not always consistent from fault to fault. This adds complexity to our understanding of frictional heating alongside noting the care needed if we are to use Raman as a geothermometer (a method of working out how hot a rock got in the past) in faulted rocks.

1. Introduction

The molecular structure of organic carbon in rocks is known to be influenced by peak temperature conditions and Raman spectroscopy has been widely used to assess the structural order of organic matter, and hence its thermal maturity, in a variety of geological settings. These range from burial maturation and hydrocarbon exploration, to regional metamorphism and fold/thrust belt evolution (Beyssac et al., 2002; Henry et al., 2018; Jehlička & Benny, 1992; Kedar et al., 2020; Lahfid et al., 2010; Liu et al., 2013; Muirhead et al., 2018, 2020; Muirhead, Parnell, et al., 2017; Rahl et al., 2005; Schito & Corrado, 2018; Schito et al., 2017, 2019; Wopenka & Pasteris, 1993). Calibration curves and burial models are typically used in these geological settings to determine temperatures from Raman spectra. In contrast the application of Raman spectroscopy to faults and shear zones (Hirono et al., 2015; Ito et al., 2017; Kedar et al., 2020; Kuo et al., 2018; Mukoyoshi et al., 2018) is only relatively recent, and debate continues over the impact on Raman spectral shifts and the drivers of these Raman parameter changes. Previous work has focused on using Raman spectroscopy to estimate the maximum temperature of organic matter due to frictional heating along faults or shear surfaces (Hirono et al., 2015; Ito et al., 2017; Kaneki et al., 2018; Kuo et al., 2017, 2018; Mukoyoshi et al., 2018). Frictional heating (or evidence for) continues to be an important topic in fault and earthquake mechanics (Fulton et al., 2013; Kanamori et al., 2000; Lachenbruch & Sass, 1980; Rice, 2006; Rowe & Griffith, 2015; Sibson et al., 1975). There have been several recent applications of organic thermal

© 2021. The Authors.

This is an open access article under the terms of the [Creative Commons Attribution License](https://creativecommons.org/licenses/by/4.0/), which permits use, distribution and reproduction in any medium, provided the original work is properly cited.

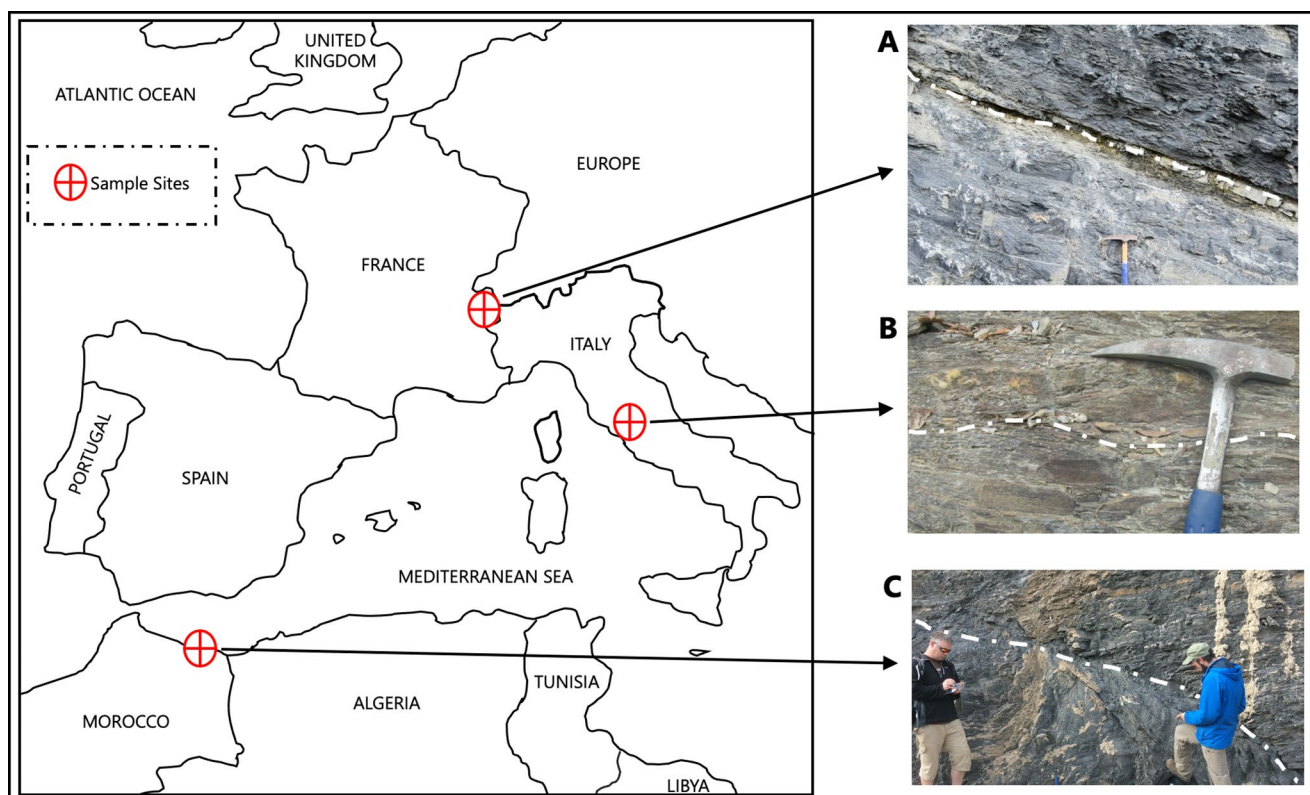


Figure 1. Location of sample sites with representative field photos showing sampled fault surfaces. (a) Salvadon Thrust: samples taken from thrust surface (white dashed line) and 20 m below; (b) one of the sample localities from Tuscany: samples taken from fault plane (white dashed line) and 20 cm away; (c) one of the sample localities from the Internal Rif, Morocco: samples taken from shear surface and 2 m below.

maturity parameters in faulted regimes (Coffey et al., 2019; Fulton & Harris, 2012; O'Hara et al., 2006; Polissar et al., 2011; Rabinowitz et al., 2020; Sakaguchi et al., 2011; Savage & Polissar, 2019; Savage et al., 2014, 2018). However the impact of frictional heating on Raman spectral shifts is still not well constrained. Other potential influences on Raman spectra in faulted samples include: strain (Kedar et al., 2020), burial depth (Schito et al., 2017) and hydrothermal alteration (Kirilova et al., 2018); as well as the influence of carbonaceous material type (Henry et al., 2018); and the interplay of these elements. Here we are not focused on discriminating between these influences, however we aim to add to the published literature on Raman spectral shifts in faulted rocks, comparing our work with previously published studies to document the range in Raman spectral shifts with a view to informing future work in this area.

In this study, we document Raman spectral shifts in faulted, and adjacent unfaulted, samples from three exhumed fault zones. The three study area locations represent different scales and types of fault zone (shear zones; discrete faults) with a range of maximum burial depths from 6 to 8 km, with the aim of expanding existing Raman spectral data across fault zones. We compare the observed Raman spectral shifts between adjacent faulted and unfaulted rocks at each locality, and compare our results with existing published data on faulted samples. Finally, we discuss the implications for carbon crystallinity and nanostructure related to fault zone deformation.

2. Geological Context

Samples were collected from three study areas (Figure 1): the Haut Giffre in the French Alps; the Monti Romani in Tuscany, Italy; and the Internal Rif in Morocco. These settings were selected to provide a broad range in sedimentary rock burial depths and hence metamorphosed and unmetamorphosed organic matter in differing geological settings, the details of which are expanded on below.

2.1. Carbonate Thrust Stack, Haute Giffre, French Alps

The Haut Giffre, western France, is a mountainous area comprising over 3 km of thrust-stacked Mesozoic carbonate stratigraphy. The two sampling localities are located on a single thrust, referred to as the Salvadon Thrust, which ramps upwards through Bajocian to Senonian stratigraphy. At the first locality (Salvadon), the thrust crops out along the length of a north-facing cliff. Here, organic-rich Valanginian (133–140 Ma) shale lies in footwall and is juxtaposed against the Tithonian (145–152 Ma) limestone within the hanging wall. One sample was collected from the Valanginian footwall at 20 m below the thrust plane (sample name: ST20) with a second sample taken from the thrust plane itself (ST0). The thrust zone thickness (in these cases typically damage zones) varies between 5 and 10 cm. The second locality (Rocher Blanc) is on the same thrust, but located toward the trailing thrust tip, where displacement is around 100 m. Here, Bajocian marls are thrust onto Oxfordian shales, but the deformation is accommodated by a series of thrust splays instead of the single discrete fault plane seen at the Salvadon locality. Samples were collected as per the procedure for the Salvadon Thrust samples: thrust plane (sample names: RB6 & RB8) and at 0.5 m (RB3) and 10 m (RB5) away from the thrust plane. The thrust zone thickness is 10 cm at most. These samples are located in the same general area of the Haut Giffre, discussed in Kedar et al. (2020), but not from the same site as that study was concerned with a wider deformation zone.

2.2. Metamorphic Units of Monti Romani, Tuscany, Italy

Exhumed metamorphic units made up of Paleozoic-Mesozoic successions of the Adria margin (Vai & Martini, 2001) represent the distinctive signature of the inner Northern Apennines fold-and-thrust belt. The Paleozoic samples analyzed belong to the southernmost outcrop of this metamorphic backbone of the Northern Apennines (Verrucchi & Minissale, 1995) and are derived from the low-grade litho-stratigraphical units “Roccaccia di Montauto Quartzite and Phyllite.” Samples were derived from two localities of graphitic metapelites at Ponte San Pietro, where the rock fabric is characterized by a well-developed phyllitic cleavage oriented NNW-SSE. Successions experienced greenschist alpine regional metamorphism (Moretti et al., 1990).

Samples were collected on the fault plane of each sample and at 20, 50, and 60 cm from the faults, sample names SZT 6 & 7; SZT 10 & 12; SZT 8 & 11 respectively. The fault zone thicknesses is less than 1 cm for sample SZT 6, between 2 and 3 cm in sample SZT 11, between 1 and 2 cm in sample SZT 8, about 5 cm in sample MAROC 16.1 and less than 1 cm in sample MAROC 17.1.

2.3. Internal Zone of the Rif Chain, Northern Morocco

The Internal Zone of the Rif chain, in Northern Morocco, comprises continental tectonic units outlined below. According to their grade of Alpine metamorphism, two distinctive complexes are recognized that form the upper and lower plates of a metamorphic core complex (Leprêtre et al., 2018). The lower plate corresponds to the Sebtide units mainly made up of relatively deep crustal rocks, associated with mantle peridotites. The upper plate consists of the Ghomaride units, that comprise Paleozoic successions affected by Variscan metamorphism (Chalouan et al., 2008), partly superimposed by weak Alpine recrystallization (Michard et al., 2006) and their Mesozoic-Cenozoic cover. Samples analyzed derive from the lowest unit among the Gomarides (namely Akaili) cropping out north of the city of Oued-Laou, where the Paleozoic succession spans the Ordovician and Carboniferous (Chalouan et al., 2008). Ghomarides rocks in this locality suffered a thermal event due to emplacement of the Beni-Boussera peridotite at 28 My that superimposed on the regional metamorphism experienced during the Variscan cycle (Michard & Chalouan, 1991). A description of Raman spectra of the metamorphosed carbonaceous material at this site can be found in Negri et al. (2004).

The selected samples were collected at the shear surface for MAROC 16.1f and 2 m away from the shear at MAROC 16.1; shear surface for MAROC 17.1f and 5 m away for MAROC 17.1. The thicknesses of these shear zones are 5 cm (MAROC 16.1) and less than 1 cm (MAROC 17.1).

2.4. Published Work

We compare our Raman spectra to previously published work on natural fault rocks and experimentally deformed rocks (Hirono et al., 2015; Ito et al., 2017; Kouketsu et al., 2017; Kuo et al., 2017, 2018). The data from Ito et al. (2017) come from a pseudotachylite bearing fault zone in the Shimanto accretionary complex of Skikoku, southwest Japan and an experimentally derived pseudotachylite from argillite collected from the same area; the data from Kuo et al. (2018) was derived from experimental graphitization in a rotary shear experiment (see Di Toro et al., 2010) of fault breccia derived from 589 m depth as part of the Wenchuan Earthquake Fault Scientific Drilling – 1 project (Kuo et al., 2018). Samples from Hirono et al. (2015) were collected to study the mechanism of fault lubrication during the 1999 Chi-Chi earthquake in Taiwan. Finally, Kouketsu et al. (2017) performed micro-Raman analyses on natural and experimentally fault rocks from the Longmenshan fault zone between the Tibetan Plateau and the Sichuan Basin.

In the work of Hirono et al. (2015) and Ito et al. (2017) natural and experimental samples derived from sedimentary rocks, while samples in Kuo et al. (2018) and Kouketsu et al. (2017) experienced low-grade metamorphism.

3. Raman Spectroscopy of Carbon

Fossil carbonaceous materials within rocks undergo a complex series of reactions when thermally altered, which involve both the formation and reordering of aromatic subunits toward stacked layers such as graphite. Raman spectroscopy has been widely used (Beysac et al., 2002; Ferrari & Robertson, 2001; Knight & White, 1989; Landis, 1971; Nemanich & Solin, 1979; Tuinstra & Koenig, 1970) as a powerful, non-destructive tool for evaluating the characterization and thermal alteration of diverse forms of carbonaceous matter (crystalline, nanocrystalline, amorphous). Measurements are mainly based on two broad first order Raman bands (spectral peaks) at $\sim 1,585\text{ cm}^{-1}$ (the graphite peak, G) and $\sim 1,350\text{ cm}^{-1}$ (the disorder peak, D). These bands represent the inelastic scattering (Stokes Raman scattering) produced by electronic and photonic induced laser irradiation. Due to the physical properties of carbonaceous materials that are based on the hybridized atomic orbital configuration of carbon atoms (Robertson, 1991), the shape and relative intensities of the D and G bands reflect the ratio of sp^2 (graphite-like, trigonal planar symmetry) and sp^3 (diamond-like, tetrahedral symmetry) carbon bonds (Robertson, 1991). The G band is assigned to the in-plane vibration of the carbon atoms in the graphene sheets and the D band either by double resonant Raman scattering or has been related to the ring breathing vibration in the graphite sub-unit or polycyclic aromatic compounds (Castiglioni et al., 2004; Di Donato et al., 2004; Lünsdorf, 2016; Negri et al., 2004).

The $\sim 1,585\text{ cm}^{-1}$ graphite peak is a composite of several Raman bands at $\sim 1,615\text{ cm}^{-1}$, $\sim 1,598\text{ cm}^{-1}$, and $\sim 1,545\text{ cm}^{-1}$ (D2, G, D3 respectively). In disordered materials, these bands are treated as one spectral peak, since it is not possible to separate the G and D2 bands in poorly organized carbon or low-grade rocks (Beysac et al., 2002). Raman spectral parameters in this study follow those outlined by Marshall et al. (2012) and Quirico et al. (2009) and fitting procedures follow those outlined in Bonal et al. (2006).

Several Raman parameters have been developed over the past few decades that involve measurements made on Raman spectral peaks. Wopenka and Pasteris (1993) measured the position and width of the G peak at $\sim 1,585\text{ cm}^{-1}$ for a suite of metamorphic zones. Increased thermal maturation leads to the structural reordering of carbonaceous materials, with an increase in the proportion of aromatic carbon, in turn narrowing the G band and shifting it closer toward lower wavenumbers. If samples are graphitic, narrowing remains similar but G peak position shifts downwards to $\sim 1,598\text{ cm}^{-1}$. It is important to note that in amorphous carbon (*a-C*), initial development of a D band indicates ordering, whereas in graphitic carbon (*ta-C*), the presence of a D band indicates disorder, so Raman parameters must be interpreted with respect to any known information about the carbon feedstock (Ferrari & Robertson, 2001).

Two D/G-peak ratios are also commonly used: I_D/I_G (intensity), and A_D/A_G (area) (see Figure 2a for summary of Raman spectral parameters). Both ratios are highly sensitive to thermal maturation and increased structural ordering (Bonal et al., 2006; Busemann et al., 2007; Marshall et al., 2012; Quirico et al., 2009; Yui et al., 1996) and can be used to reveal differences in thermal alteration of carbonaceous materials (Jehlička & Bény, 1992; Pasteris & Wopenka, 1991). However, the relationship between these ratios and temperature

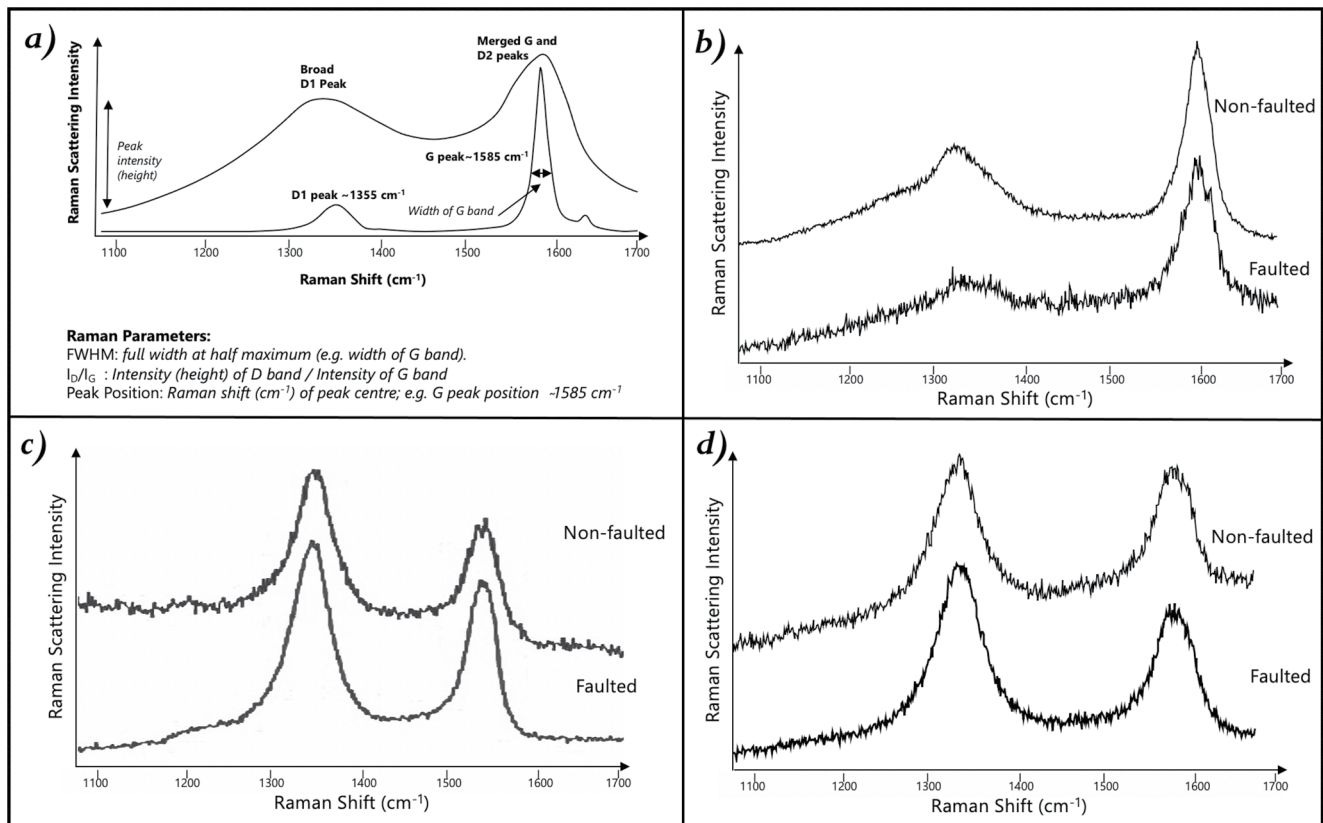


Figure 2. Summary of Raman spectral features used in this study (a). Representative stacked first order Raman spectra: (b) the Haut Giffre in the French Alps; (c) Monti Romani Tuscany, Italy; (d) Internal Rif, Morocco.

is not linear, or indeed simple. In general, I_D/I_G (intensity) would be expected to decrease with increasing structural ordering (Pasteris & Wopenka, 1991), but in fact in early stage thermal alteration can raise the I_D/I_G parameter (Muirhead et al., 2012; Rouzaud et al., 1983).

Raman spectroscopy has proven a useful tool for the evaluation of low-level thermal alteration at temperatures lower than 300°C (Muirhead et al., 2020; Schito et al., 2017), alongside basic kinetic modeling of heating adjacent to intrusions, prediction of potential oil window location and source rock generation potential (Muirhead, Bowden, et al., 2017; Muirhead et al., 2012, 2018). In diagenesis, many authors have demonstrated that Raman parameters related to the position (Kelemen & Fang, 2001; Liu et al., 2013; Lupoi et al., 2017; Mumm & Inan, 2016; Wilkins et al., 2014) or to the area/width ratios of the D and G bands (Guedes et al., 2010, 2012; Hinrichs et al., 2014; Lünsdorf, 2016; Muirhead, Bowden, et al., 2017; Muirhead, Parnell, et al., 2017; Quirico et al., 2009; Schito & Corrado, 2018; Schito et al., 2017; Schmidt et al., 2017) vary as a function of thermal maturity and/or different organofacies (Schito et al., 2019) in the immature-to-mid-mature stages of hydrocarbon generation.

Here we build on previous work of Raman spectroscopy applied to geological samples to better understand geological process to fault zones in carbonaceous rocks. The purpose of this study is to document variations in Raman spectra signatures within representative non-faulted and faulted samples from three study areas. Future work will aim to discriminate in detail the processes that may be controlling these Raman responses in faulted samples.

4. Methodology

4.1. Sample Selection

Representative faulted and non-faulted samples were collected as rock chips. Care was taken to avoid cases of hydrothermal alteration and mineralization. The areas were also checked to ensure no impact from any intrusive igneous bodies (example exposure and representative first order Raman spectra are shown in Figures 1 and 2). Organic matter within the samples were targeted for analysis using the Raman microscope on rock samples.

4.2. Raman Spectroscopy

Raman measurements were performed independently by two different laboratories to reduce the reliance on one user, analytical set-up and operator bias. At the University of Aberdeen, analyses were conducted on a Renishaw inVia reflex Raman spectrometer. A Leica DMLM reflected light microscope was used to focus the Ar⁺ green laser (wavelength 514.5 nm). The laser spot size was approximately 1–2 μm and laser power between 10%–50% (<13 mW power at the sample). The scattered light was dispersed and recorded by means of a CCD (Charge Coupled Device) detector. Data were collected between 1100 cm^{-1} and 1700 cm^{-1} with a spectral resolution less than 3 cm^{-1} . The duration of accumulations was typically up to 10 s for between 3 and 5 accumulations.

The Renishaw WiRE 3.0 curve-fit software was used for spectral deconvolution. Smoothing and baseline extractions, using a cubic spline interpolation, were performed on each sample. To ensure reproducibility and the removal of any background signal, data were extracted (using Gaussian curve fitting) from at least three deconvolution cycles per sample. Peak position and peak width (defined as full width at half maximum, FWHM) were recorded as wavenumbers (cm^{-1}), indicating the change in vibrational frequency (stretching and breathing) of the Raman-active carbon molecules. Spectral processing and deconvolution was applied to measure peak areas, with composite G and D bands used to calculate I_D/I_G ratios as outlined in Muirhead et al. (2012, 2018), Muirhead, Parnell, et al. (2017), and Kedar et al. (2020).

At the University of Roma Tre, micro-Raman spectroscopy was carried out using a Horiba Jobin-Yvon LabRam Microscope XploRATM system in a backscattering geometry, in the range of 700–2,300 cm^{-1} using a 600 grooves/mm spectrometer gratings and CCD detector. The instrument is equipped with 50 \times and 100 \times objective lens (\sim 2 μm diameter at the laser spot). An excitation wavelength of 532 nm from an Ar⁺ laser at a power of 40 mW was reduced by two orders of magnitude using optical filters (i.e., laser power on the sample is 0, 4 mW). Raman backscattered radiation was recorded for an integration time of 20 s for six repetitions, with spectral analysis after Schito and Corrado (2018).

5. Results

Representative stacked first order Raman bands are presented in Figures 2b–2d. Deconvolved Raman spectral parameters exhibit a shift in G band wavenumbers (peak position, W_G [cm^{-1}]) and G band width (FWHM) (Figure 3), from non-faulted and faulted samples. The Moroccan and Italian samples show a decrease in both FWHM and peak position from non-faulted to faulted samples. Similarly, one set of French samples (Salvador thrust) exhibit the same trend. However, further along the same thrust, at the Rocher Blanc locality, the faulted samples have higher peak positions and widths. We also plot data from Hirono et al. (2015), who report Raman spectra from drilling of the Chelungpu Fault, Taiwan. These data exhibit a decrease in FWHM but not peak position from unfaulted to faulted materials. Table 1 summarizes the Raman spectral responses.

Despite there being clear differences in the intensity and direction of response (Figure 3), there is a shift across all sample sites, consistent with a change in the nanostructural order of organic materials (Beyssac et al., 2002; Muirhead, Parnell, et al., 2017; Wopenka & Pasteris, 1993). Each sample set clusters within isolated regions in the crossplot; France (top left), Morocco (middle) and Italy (bottom right). This is likely a product of differences linked to the nature of the organic materials analyzed and different organofacies whereby the initial spectral signal is unique to the rock. Regardless of the starting material, there is a shift

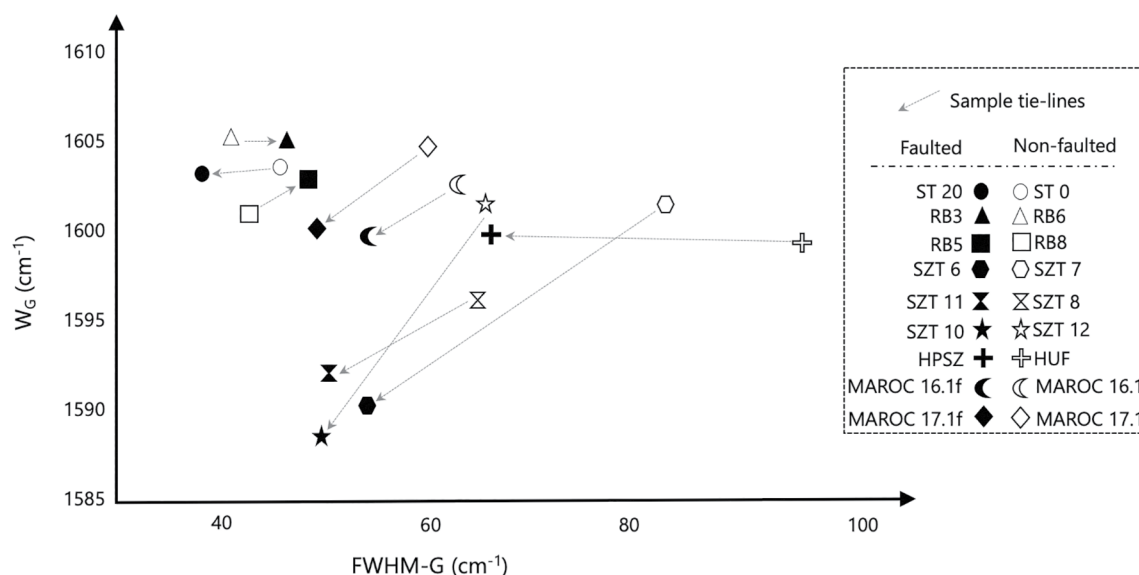


Figure 3. Crossplot of G band peak position (W_G [cm⁻¹]) against G band full width at half maximum (FWHM). Open symbols are non-faulted; shaded symbols are faulted. RB = Rocher Blanc; ST = Salvadon Thrust (both from the French Alps). SZT = Shear Zone Tuscanny, Monti Romani, Italy. MAROC = Internal Rif, Morocco. HPSZ = Hirono et al. (2015) Primary Slip Zone; HUF = Hirono et al. (2015) unfaulted.

from non-faulted to faulted samples, demonstrating that the faulting process affects the carbon structure. Peak intensity ratios ($I[d]/I[g]$) also undergo a marked shift between non-faulted and faulted samples (Figure 3) but these do not necessarily relate to the direction of change in FWHM and peak position. For example, both the French Salvadon thrust sample pairs shows a decrease in FWHM and peak position, much like the Italian and Moroccan samples, yet $I[d]/I[g]$ is higher on the fault plane than the non-faulted sample, contrary to those of the Italian and Moroccan sites. Inconsistency in the $I[d]/I[g]$ shift direction has already been observed in apparently unfaulted rocks. Studies (Busemann et al., 2007; Yui et al., 1996) indicate

Table 1
Summary of Raman Spectral Results for Each Sample in This Study

Sample name	Sample location	W_G	FWHM-G	I_D/I_G (mean)
MAROC 16.1	Internal Rif, Morocco	1603.5	62	Faulted: 2.0
MAROC 16.1f		1,599	54	non-faulted: 1.25
MAROC 17.1		1,605	60	
MAROC 17.1f		1,600	48	
RB 3	Rocher Blanc, Haut Giffre, French Alps	1,605	56	Faulted: 0.51
RB 5		1,603	47	non-faulted: 0.55
RB 6		1,605	41	
RB 8		1,601	42	
ST 0	Salvadon, Haut Giffre, French Alps	1,604	45	Faulted: 0.25
ST 20		1603.5	38	non-faulted: 0.50
SZT 10	Monti Romani, Tuscanny, Italy	1,589	49	Faulted: 1.50
SZT 11		1591.5	50	non-faulted: 0.95
SZT 12		1,602	66	
SZT 6		1,590	55	
SZT 7		1,602	82	
SZT 8		1,596	64	

Note. FWHM, full width at half maximum.

a decrease in the I_D/I_G ratio being indicative of greater nanostructural ordering due to progressive thermal maturation, while others (Muirhead, Bowden, et al., 2017; Muirhead et al., 2012; Rouzaud et al., 1983; Schito & Corrado, 2018) suggest that in the early stages of thermal maturation, typical of low-grade metamorphic settings the reverse is true, and I_D/I_G increases with maturation. In Figure 4, we have also plotted data from four other studies of faulted rock: Hirono et al. (2015), also plotted in Figure 3, and data from Ito et al. (2017), Kuo et al. (2018), and Kouketsu et al. (2017). The Hirono et al. (2015) and Ito et al. (2017) results show similar trends in $I[D]/I[G]$ shift direction to our case study sites from Italy and Morocco (an increase through faulting), whereas the Kuo et al. (2018) samples show a shift comparable to the French Alps samples (a decrease) (Figure 4). From the evidence presented, we can infer that, while faulting consistently has a direct effect on the peak intensity (I_D/I_G) ratio, the exact nature of this effect appears to depend on the local geological context (see below).

6. Discussion

Based on our observations, we can state that the faulting process change the nanostructural order of the organic carbon in the samples. The mechanisms for driving these changes remain unknown, but given the differences in Raman spectral shift observed we suggest that the mechanisms for nonstructural change may differ between samples. Several key processes occurring on these faults could impact the carbon nanostructure. We consider here how the changes to the Raman spectra we observe may be influenced by different processes. In summary, our discussions are inconclusive and our final discussion point highlights the need for more work in this area.

6.1. G-Peak FWHM and Wavenumber

Heating is interpreted as lowering the G-peak width and wave number (Beyssac et al., 2002; Muirhead, Parnell, et al., 2017; Wopenka & Pasteris, 1993). In Figure 3, the dominant trend is a reduction in G-peak width and wavenumber in faulted samples. This change could be attributed to increased thermal maturity of carbonaceous material on the fault compared to the surrounding rock due to frictional heating. However, this trend is not consistent, samples RB5 & RB8 and RB3 & RB6 (Figure 3) show the opposite trend, suggesting that if frictional heating does have an effect, it is not the only factor at play. Raman spectral shifts on a single fault at a regional scale, are also observed in our data. The French Salvadon thrust, is a regional thrust, which has several hundred meters of displacement and two different lithologies are juxtaposed across the fault plane. However, toward the fault tip on the same thrust, 1 km along strike, the Rocher Blanc sample site, the displacement is around an order of magnitude less, and the fault plane is less well defined, with deformation distributed across a series of fault splays and linked shear zones within the same lithology. On this one structure the Raman response to faulting is observed to vary between these two sample sites, with G peak FWHM increasing in the Rocher Blanc faulted sample and decreasing in the Slavadon faulted sample (Figure 3).

6.2. I_D/I_G Intensity Ratios

Figure 4 demonstrates a shift in peak intensity ratios when moving from non-faulted to faulted samples, but the direction of this shift varies, and does not always match with the direction of change in G FWHM or peak position. This also suggests that the processes contributing to nanostructural changes in carbon along these faults are more complex than temperature elevation due to frictional heating. Under regional metamorphic conditions the I_D/I_G variation with temperature can be summarized in three main patterns: in diagenesis up to 200°C no substantial variation is observed (Lünsdorf, 2016; Schito et al., 2017), while the parameters start to increase from 250 to about 375°C and at higher temperatures progressively decrease and disappear approaching graphitic carbon. A frictional heating temperature increase would explain the increase in I_D/I_G in the Italian and Moroccan samples, as at low metamorphic grades a temperature increase equates to an increase in I_D/I_G (Lahfid et al., 2010). The French samples underwent similar low-grade metamorphism, so we would expect frictional heating to produce the same response, but a decrease in I_D/I_G is observed. Alternative explanations must be invoked to explain this decrease. On samples in a nearby distributed shear zone in the sheared overturned limb of a recumbent fold Kedar et al. (2020) suggest that sample strain may cause observed decreases in I_D/I_G . On the more discrete fault planes sampled here, higher in

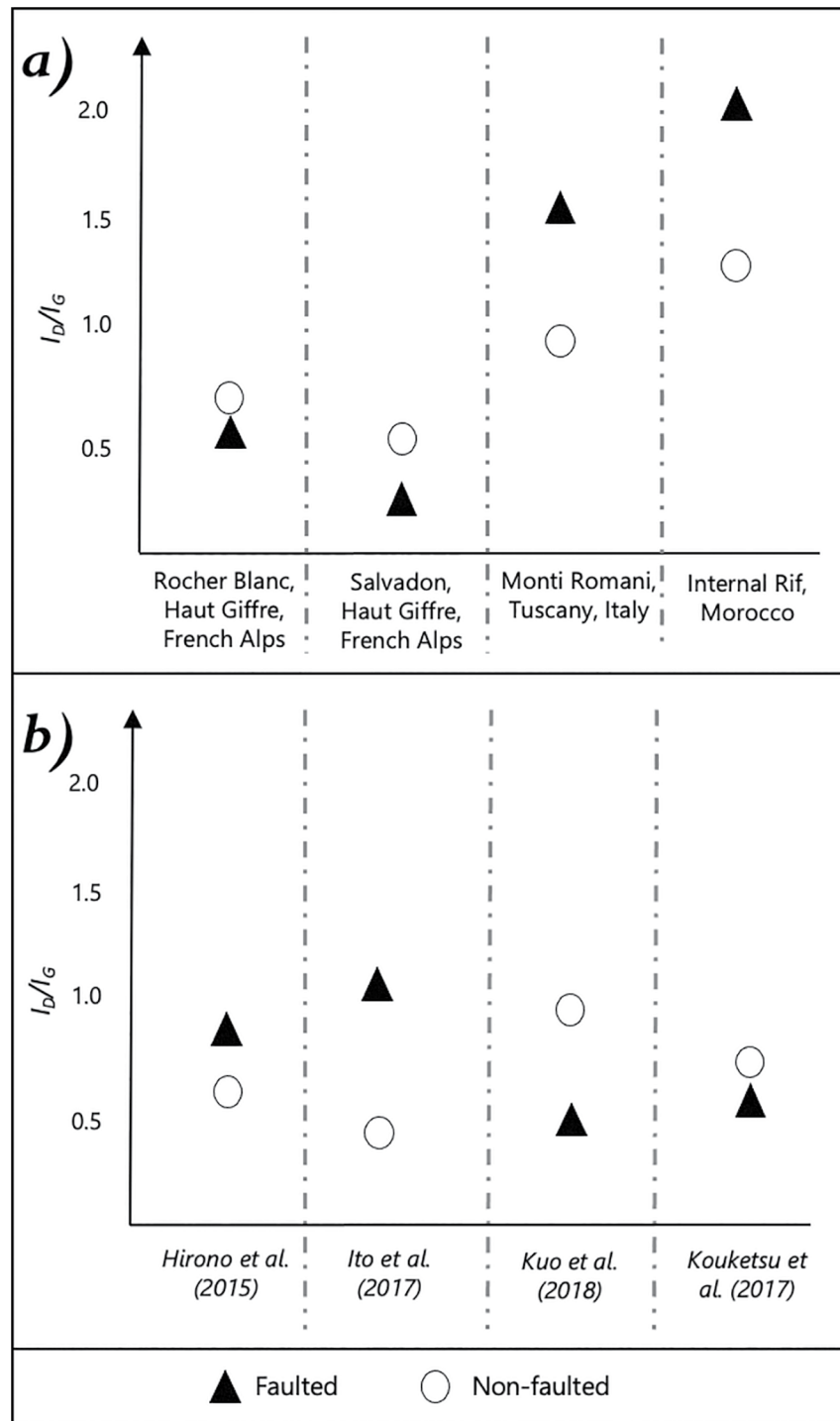


Figure 4. (a) I_D/I_G ratios from samples in this study; (b) I_D/I_G ratios from published works. I_D/I_G ratios are presented for both faulted and non-faulted samples on the y-axes with each sample site/previous study presented on the x-axis. Dashed lines delineate each study. The inconsistency of the I_D/I_G ratios is clear from both the work in this study and those of others.

the stratigraphic succession, frictional heating and strain may be operating together. There is also evidence that under different heating conditions (e.g., fast heating near intrusions) I_D/I_G can show different behavior when maturation starts from an immature or an already mature organic material (Muirhead, Bowden, et al., 2017; Muirhead, Parnell, et al., 2017). There is evidence from other studies (Henry et al., 2018; Muir-

head, Bowden, et al., 2017; Muirhead, Parnell, et al., 2017; Quirico et al., 2009) that changes to carbon nanostructure may also be dependent on the starting type of the carbonaceous material. Finally, in the case of frictional heating on a fault surface, experimental work is not conclusive for I_D/I_G variation (Ito et al., 2017; Kouketsu et al., 2017; Kuo et al., 2018).

6.3. Constraining the Underpinning Process of Nanostructural Change in Faulted Samples

Experimental work has attempted to constrain Raman response (e.g., Hirono et al., 2015; Kirilova et al., 2018; Kuo et al., 2018) to faulting but these experiments did not uncouple temperature resulting from frictional heating from sample strain. The experimental work of Hirono et al. (2015) suggest that the Raman spectra changes in their fault samples from Taiwan are the result of frictional heating rather than deformation mechanisms; whereas Kirilova et al. (2018) suggest in their case that brittle deformation is responsible for Raman spectra shifts. Isolating the different possible variables that may influence nanostructural change in carbon during faulting is a remaining challenge. It is clear from the data presented here that, in order to address that challenge, more systematic sampling is needed across fault zone study areas, if Raman spectral parameters are going to be used in faulted samples to better understand Earth processes.

7. Conclusions

Raman spectroscopy was successfully applied to a suite of faulted and non-faulted samples showing that:

1. Some samples exhibit a lowering of the G peak position and width in faulted samples, but some samples show the reverse trend.
2. There is a shift in the I_D/I_G ratios, between paired faulted and unfaulted samples, but no consistent trend.
3. Raman spectra are influenced by faulting in natural, as well as experimental rock samples and thus caution must be applied when interpreting Raman spectra to derive burial depths from palaeotemperatures in faulted samples.
4. Further work is needed to better understand the processes that result in modified spectra in faulted samples.

Data Availability Statement

New Raman results for this study are archived in Zenodo under: <https://doi.org/10.5281/zenodo.4302176>. Further Raman data for this research are included in the following papers: Hirono et al. (2015), Ito et al. (2017), Kouketsu et al. (2017), and Kuo et al. (2018).

Acknowledgments

The authors thank Colin Taylor at UoA for help in sample preparation. This study was supported by the School of Geosciences at the University of Aberdeen and in part by the NERC Centre for Doctoral Training in Oil & Gas (Grant Number: NE/R01051x/1).

References

- Beysnac, O., Goffé, B., Chopin, C., & Rouzaud, J. N. (2002). Raman spectra of carbonaceous material in metasediments: A new geothermometer. *Journal of Metamorphic Geology*, 20(9), 859–871. <https://doi.org/10.1046/j.1525-1314.2002.00408.x>
- Bonal, L., Quirico, E., Bourot-Denise, M., & Montagnac, G. (2006). Determination of the petrologic type of CV3 chondrites by Raman spectroscopy of included organic matter. *Geochimica et Cosmochimica Acta*, 70(7), 1849–1863. <https://doi.org/10.1016/j.gca.2005.12.004>
- Busemann, H., Alexander, M. O., & Nittler, L. R. (2007). Characterization of insoluble organic matter in primitive meteorites by micro-Raman spectroscopy. *Meteoritics & Planetary Sciences*, 42(7–8), 1387–1416. <https://doi.org/10.1111/j.1945-5100.2007.tb00581.x>
- Castiglioni, C., Tommasini, M., & Zerbi, G. (2004). Raman spectroscopy of polyconjugated molecules and materials: Confinement effect in one and two dimensions. *Philosophical Transactions of the Royal Society of London. Series A: Mathematical, Physical and Engineering Sciences*, 362, 2425–2459. <https://doi.org/10.1098/rsta.2004.1448>
- Chalouan, A., Michard, A., El Kadiri, K., Negro, F., De Lamotte, D. F., Soto, J. I., & Saddiqi, O. (2008). The Rif belt. In *Continental evolution: The geology of Morocco* (pp. 203–302). Springer. https://doi.org/10.1007/978-3-540-77076-3_5
- Coffey, G. L., Savage, H. M., Polissar, P. J., Rowe, C. D., & Rabinowitz, H. S. (2019). Hot on the trail: Coseismic heating on a localized structure along the Muddy Mountain fault, Nevada. *Journal of Structural Geology*, 120, 67–79. <https://doi.org/10.1016/j.jsg.2018.12.012>
- Di Donato, E., Tommasini, M., Fustella, G., Brambilla, L., Castiglioni, C., Zerbi, G., et al. (2004). Wavelength-dependent Raman activity of D2h symmetry polycyclic aromatic hydrocarbons in the D-band and acoustic phonon regions. *Chemical Physics*, 301, 81–93. <https://doi.org/10.1016/j.chemphys.2004.02.018>
- Di Toro, G., Niemeijer, A., Tripoli, A., Nielsen, S., Di Felice, F., Scarlato, P., et al. (2010). From field geology to earthquake simulation: A new state-of-the-art tool to investigate rock friction during the seismic cycle (SHIVA). *Rendiconti Lincei*, 21(1), 95–114. <https://doi.org/10.1007/s12210-010-0097-x>

- Ferrari, A. C., & Robertson, J. (2001). Resonant Raman spectroscopy of disordered, amorphous and diamond-like carbon. *Physical Review B*, 64, 075414. <https://doi.org/10.1103/physrevb.64.075414>
- Fulton, P. M., Brodsky, E. E., Kano, Y., Mori, J., Chester, F., Ishikawa, T., et al. (2013). Expedition 343, 343T, and KR13-08 Scientists Low coseismic friction on the Tohoku-Oki fault determined from temperature measurements. *Science*, 342(6163), 1214–1217. <https://doi.org/10.1126/science.1243641>
- Fulton, P. M., & Harris, R. N. (2012). Thermal considerations in inferring frictional heating from vitrinite reflectance and implications for shallow coseismic slip within the Nankai Subduction Zone. *Earth and Planetary Science Letters*, 335, 206–215. <https://doi.org/10.1016/j.epsl.2012.04.012>
- Guedes, A., Valentim, B., Prieto, A., & Noronha, F. (2012). Raman spectroscopy of coal macerals and fluidized bed char morphotypes. *Fuel*, 97, 443–449. <https://doi.org/10.1016/j.fuel.2012.02.054>
- Guedes, A., Valentim, B., Prieto, A. C., Rodrigues, S., & Noronha, F. (2010). Micro-Raman spectroscopy of collotelinite, fusinite and macrinite. *International Journal of Coal Geology*, 83, 415–422. <https://doi.org/10.1016/j.coal.2010.06.002>
- Henry, D. G., Jarvis, I., Gillmore, G., Stephenson, M., & Emmings, J. F. (2018). Assessing low-maturity organic matter in shales using Raman spectroscopy: Effects of sample preparation and operating procedure. *International Journal of Coal Geology*, 191, 135–151. <https://doi.org/10.1016/j.coal.2018.03.005>
- Hinrichs, R., Brown, M. T., Vasconcellos, M. A., Abrashev, M. V., & Kalkreuth, W. (2014). Simple procedure for an estimation of the coal rank using micro-Raman spectroscopy. *International Journal of Coal Geology*, 136, 52–58. <https://doi.org/10.1016/j.coal.2014.10.013>
- Hirono, T., Maekawa, Y., & Yabuta, H. (2015). Investigation of the records of earthquake slip in carbonaceous materials from the Taiwan Chelungpu fault by means of infrared and Raman spectroscopies. *Geochemistry, Geophysics, Geosystems*, 16(5), 1233–1253. <https://doi.org/10.1002/2014gc005622>
- Ito, K., Ujiie, K., & Kagi, H. (2017). Detection of increased heating and estimation of coseismic shear stress from Raman spectra of carbonaceous material in pseudotachylytes. *Geophysical Research Letters*, 44(4), 1749–1757. <https://doi.org/10.1002/2016gl072457>
- Jehlička, J., & Bény, C. (1992). Application of Raman microspectrometry in the study of structural changes in Precambrian kerogens during regional metamorphism. *Organic Geochemistry*, 18(2), 211–213.
- Kanamori, H., Heaton, T. H., & Rundle, J. B. (2000). *Microscopic and macroscopic physics of earthquakes* (Vol. 120, pp. 147–163). Geophysical Monograph-American Geophysical Union. <https://doi.org/10.1029/gm120p0147>
- Kaneki, S., Ichiba, T., & Hirono, T. (2018). Mechanochemical effect on maturation of carbonaceous material: Implications for thermal maturity as a proxy for temperature in estimation of coseismic slip parameters. *Geophysical Research Letters*, 45(5), 2248–2256. <https://doi.org/10.1002/2017gl076791>
- Kedar, L., Bond, C. E., & Muirhead, D. (2020). Carbon ordering in an aseismic shear zone: Implications for Raman geothermometry and strain tracking. *Earth and Planetary Science Letters*, 549, 116536. <https://doi.org/10.1016/j.epsl.2020.116536>
- Kelemen, S., & Fang, H. (2001). Maturity trends in Raman spectra from kerogen and coal. *Energy & Fuels*, 15, 653–658. <https://doi.org/10.1021/ef0002039>
- Kirilova, M., Toy, V. G., Timms, N., Halpenny, A., Menzies, C., Craw, D., et al. (2018). Textural changes of graphitic carbon by tectonic and hydrothermal processes in an active plate boundary fault zone, Alpine Fault, New Zealand. *Geological Society, London, Special Publications*, 453(1), 205–223. <https://doi.org/10.1144/sp453.13>
- Knight, D. S., & White, W. B. (1989). Characterization of diamond films by Raman spectroscopy. *Journal of Materials Research*, 4, 385–393. <https://doi.org/10.1557/jmr.1989.0385>
- Kouketsu, Y., Shimizu, I., Wang, Y., Yao, L., Ma, S., & Shimamoto, T. (2017). Raman spectra of carbonaceous materials in a fault zone in the Longmenshan thrust belt, China; comparisons with those of sedimentary and metamorphic rocks. *Tectonophysics*, 699, 129–145. <https://doi.org/10.1016/j.tecto.2017.01.015>
- Kuo, L. W., Di Felice, F., Spagnuolo, E., Di Toro, G., Song, S. R., Aretusini, S., et al. (2017). Fault gouge graphitization as evidence of past seismic slip. *Geology*, 45(11), 979–982. <https://doi.org/10.1130/g39295.1>
- Kuo, L. W., Huang, J. R., Fang, J. N., Si, J., Song, S. R., Li, H., & Yeh, E. C. (2018). Carbonaceous materials in the fault zone of the Longmenshan fault belt: 2. Characterization of fault gouge from deep drilling and implications for fault maturity. *Minerals*, 8(9), 393. <https://doi.org/10.3390/min8090393>
- Lachenbruch, A. H., & Sass, J. H. (1980). Heat flow and energetics of the San Andreas fault zone. *Journal of Geophysical Research*, 85(B11), 6185–6222. <https://doi.org/10.1029/jb085ib11p06185>
- Lahfid, A., Beyssac, O., Deville, E., Negro, F., Chopin, C., & Goffé, B. (2010). Evolution of the Raman spectrum of carbonaceous material in low-grade metasediments of the Glarus Alps (Switzerland). *Terra Nova*, 22, 354–360. <https://doi.org/10.1111/j.1365-3121.2010.00956.x>
- Landis, C. A. (1971). Graphitisation of dispersed carbonaceous material in metamorphic rocks. *Contributions to Mineralogy and Petrology*, 30, 34–45. <https://doi.org/10.1007/bf00373366>
- Leprêtre, R., de Lamotte, D. F., Combier, V., Gimeno-Vives, O., Mohn, G., & Eschard, R. (2018). *The Tell-Rif orogenic system (Morocco, Algeria, Tunisia) and the structural heritage of the southern Tethys margin*.
- Liu, D., Xiao, X., Tian, H., Min, Y., Zhou, Q., Cheng, P., & Shen, J. (2013). Sample maturation calculated using Raman spectroscopic parameters for solid organics: Methodology and geological applications. *Chinese Science Bulletin*, 58, 1285–1298. <https://doi.org/10.1007/s11434-012-5535-y>
- Lünsdorf, N. K. (2016). Raman spectroscopy of dispersed vitrinite—Methodical aspects and correlation with reflectance. *International Journal of Coal Geology*, 153, 75–86. <https://doi.org/10.1016/j.coal.2015.11.010>
- Lupoi, J. S., Fritz, L. P., Parris, T. M., Hackley, P. C., Solotky, L., Eble, C. F., & Schlaegle, S. (2017). Assessment of thermal maturity trends in Devonian–Mississippian source rocks using Raman spectroscopy: Limitations of peak-fitting method. *Frontiers in Energy Research*, 5, 24. <https://doi.org/10.3389/fenrg.2017.00024>
- Marshall, A. O., Emry, J. R., & Marshall, C. P. (2012). Multiple generations of carbon in the Apex chert and implications for preservation of microfossils. *Astrobiology*, 12(2), 160–166. <https://doi.org/10.1089/ast.2011.0729>
- Michard, A., & Chalouan, A. (1991). The Ghomarides nappes, rif coast range, Morocco: An African terrane in the West Mediterranean alpine belt= Η παλαιozoϊκή περιοχή Ghomarides του Μαρόκου και η ένταξή της στο τεκτονικό σύστημα της Δυτικής Μεσογείου. *Δελτίον της Ελληνικής Γεωλογικής Εταιρείας*, 25(1), 117–129.
- Michard, A., Negro, F., Saddiqi, O., Bouybaouene, M. L., Chalouan, A., Montigny, R., & Goffé, B. (2006). Pressure–temperature–time constraints on the Maghrebide mountain building: Evidence from the Rif–Betic transect (Morocco, Spain), Algerian correlations, and geodynamic implications. *Comptes Rendus Geoscience*, 338(1–2), 92–114. <https://doi.org/10.1016/j.crte.2005.11.011>
- Moretti, A., Meletti, C., & Ottria, G. (1990). Studio stratigrafico e strutturale dei Monti Romani (GR-VT)-1: Dal Paleozoico all'orogenesi alpica. *Bollettino della Societa Geologica Italiana*, 109, 557–581.

- Muirhead, D. K., Bond, C. E., Watkins, H., Butler, R. W., Schito, A., Crawford, Z., & Marfino, A. (2020). Raman spectroscopy: An effective thermal marker in low temperature carbonaceous fold–thrust belts. *Geological Society, London, Special Publications*, 490(1), 135–151. <https://doi.org/10.1144/sp490-2019-27>
- Muirhead, D. K., Bowden, S. A., Parnell, J., & Schofield, N. (2017). Source rock maturation due to igneous intrusion in rifted margin petroleum systems. *Journal of the Geological Society, London*, 174, 979–987. <https://doi.org/10.1144/jgs2017-011>
- Muirhead, D. K., Duffy, M., Schofield, N., Mark, N., & Rowe, M. D. (2018). *Making oil from magma* (p. 484). Geological Society Special Publications.
- Muirhead, D. K., Parnell, J., Spinks, S., & Bowden, S. A. (2017). Characterization of organic matter in the Torridonian using Raman spectroscopy. *Geological Society, London, Special Publications*, 448, 71–80. <https://doi.org/10.1144/sp448.2>
- Muirhead, D. K., Parnell, J., Taylor, C., & Bowden, S. A. (2012). A kinetic model for the thermal evolution of sedimentary and meteoritic organic carbon using Raman spectroscopy. *Journal of Analytical and Applied Pyrolysis*, 96, 153–161. <https://doi.org/10.1016/j.jaap.2012.03.017>
- Mukoyoshi, H., Kaneki, S., & Hirono, T. (2018). Slip parameters on major thrusts at a convergent plate boundary: Regional heterogeneity of potential slip distance at the shallow portion of the subducting plate. *Earth, Planets and Space*, 70(1), 36. <https://doi.org/10.1186/s40623-018-0810-z>
- Mumm, A. S., & Inan, S. (2016). Microscale organic maturity determination of graptolites using Raman spectroscopy. *International Journal of Coal Geology*, 162, 96–107. <https://doi.org/10.1016/j.coal.2016.05.002>
- Negri, F., di Donato, E., Tommasini, M., Castiglioni, C., Zerbi, G., & Müllen, K. (2004). Resonance Raman contribution to the D band of carbon materials: Modeling defects with quantum chemistry. *Journal of Chemical Physics*, 120, 11889–11900. <https://doi.org/10.1063/1.1710853>
- Nemanich, R. J., & Solin, S. A. (1979). First and second order Raman scattering from finite-size crystals of graphite. *Physical Review B*, 20, 392–401. <https://doi.org/10.1103/physrevb.20.392>
- O'Hara, K., Mizoguchi, K., Shimamoto, T., & Hower, J. C. (2006). Experimental frictional heating of coal gouge at seismic slip rates: Evidence for devolatilization and thermal pressurization of gouge fluids. *Tectonophysics*, 424(1–2), 109–118. <https://doi.org/10.1016/j.tecto.2006.07.007>
- Pasteris, J. D., & Wopenka, B. (1991). Raman spectra of graphite as indicators of degree of metamorphism. *The Canadian Mineralogist*, 29(1), 1–9.
- Polissar, P. J., Savage, H. M., & Brodsky, E. E. (2011). Extractable organic material in fault zones as a tool to investigate frictional stress. *Earth and Planetary Science Letters*, 311(3–4), 439–447. <https://doi.org/10.1016/j.epsl.2011.09.004>
- Quirico, E., Montagnac, G., Rouzaud, J., Bonal, L., Bourot-Denise, M., Duber, S., & Reynard, B. (2009). Precursor and metamorphic condition effects on Raman spectra of poorly ordered carbonaceous matter in chondrites and coals. *Earth and Planetary Science Letters*, 287(1–2), 185–193. <https://doi.org/10.1016/j.epsl.2009.07.041>
- Rabinowitz, H. S., Savage, H. M., Polissar, P. J., Rowe, C. D., & Kirkpatrick, J. D. (2020). Earthquake slip surfaces identified by biomarker thermal maturity within the 2011 Tohoku-Oki earthquake fault zone. *Nature Communications*, 11(1), 1–9. <https://doi.org/10.1038/s41467-020-14447-1>
- Rahl, J. M., Anderson, K. M., Brandon, M. T., & Fassoulas, C. (2005). Raman spectroscopic carbonaceous material thermometry of low-grade metamorphic rocks: Calibration and application to tectonic exhumation in Crete, Greece. *Earth and Planetary Science Letters*, 240(2), 339–354. <https://doi.org/10.1016/j.epsl.2005.09.055>
- Rice, J. R. (2006). Heating and weakening of faults during earthquake slip. *Journal of Geophysical Research*, 111(B5). <https://doi.org/10.1029/2005jb004006>
- Robertson, J. (1991). Hard amorphous (diamond-like) carbons. *Progress in Solid State Chemistry*, 21(4), 199–333. [https://doi.org/10.1016/0079-6786\(91\)90002-h](https://doi.org/10.1016/0079-6786(91)90002-h)
- Rouzaud, J. N., Oberlin, A., & Beny-Bassez, C. (1983). Carbon films: Structure and microtexture (optical and electron microscopy, Raman spectroscopy). *Thin Solid Films*, 105(1), 75–96. [https://doi.org/10.1016/0040-6090\(83\)90333-4](https://doi.org/10.1016/0040-6090(83)90333-4)
- Rowe, C. D., & Griffith, W. A. (2015). Do faults preserve a record of seismic slip: A second opinion. *Journal of Structural Geology*, 78, 1–26. <https://doi.org/10.1016/j.jsg.2015.06.006>
- Sakaguchi, A., Chester, F., Curewitz, D., Fabbri, O., Goldsby, D., Kimura, G., et al. (2011). Seismic slip propagation to the updip end of plate boundary subduction interface faults: Vitrinite reflectance geothermometry on Integrated Ocean Drilling Program NanTro SEIZE cores. *Geology*, 39(4), 395–398. <https://doi.org/10.1130/g31642.1>
- Savage, H. M., & Polissar, P. J. (2019). Biomarker thermal maturity reveals localized temperature rise from paleoseismic slip along the punchbowl fault, CA, USA. *Geochemistry, Geophysics, Geosystems*, 20(7), 3201–3215. <https://doi.org/10.1029/2019gc008225>
- Savage, H. M., Polissar, P. J., Sheppard, R., Rowe, C. D., & Brodsky, E. E. (2014). Biomarkers heat up during earthquakes: New evidence of seismic slip in the rock record. *Geology*, 42(2), 99–102. <https://doi.org/10.1130/g34901.1>
- Savage, H. M., Rabinowitz, H. S., Spagnuolo, E., Aretusini, S., Polissar, P. J., & Di Toro, G. (2018). Biomarker thermal maturity experiments at earthquake slip rates. *Earth and Planetary Science Letters*, 502, 253–261. <https://doi.org/10.1016/j.epsl.2018.08.038>
- Schito, A., & Corrado, S. (2018). An automatic approach for characterization of the thermal maturity of dispersed organic matter Raman spectra at low diagenetic stages. *Geological Society, London, Special Publications*, 484, 107–109. <https://doi.org/10.1144/sp484.5>
- Schito, A., Romano, C., Corrado, S., Grigo, D., & Poe, B. (2017). Diagenetic thermal evolution of organic matter by Raman spectroscopy. *Organic Geochemistry*, 106, 57–67. <https://doi.org/10.1016/j.orggeochem.2016.12.006>
- Schito, A., Spina, A., Corrado, S., Cirilli, S., & Romano, C. (2019). Comparing optical and Raman spectroscopic investigations of phytoclasts and sporomorphs for thermal maturity assessment: The case study of Hettangian continental facies in the Holy Cross Mts.(central Poland). *Marine and Petroleum Geology*, 104, 331–345. <https://doi.org/10.1016/j.marpetgeo.2019.03.008>
- Schmidt, J. S., Hinrichs, R., & Araujo, C. V. (2017). Maturity estimation of phytoclasts in strew mounts by micro-Raman spectroscopy. *International Journal of Coal Geology*, 173, 1–8. <https://doi.org/10.1016/j.coal.2017.02.003>
- Sibson, R. H., Moore, J. M. M., & Rankin, A. H. (1975). Seismic pumping—A hydrothermal fluid transport mechanism. *Journal of the Geological Society*, 131(6), 653–659. <https://doi.org/10.1144/gsjgs.131.6.0653>
- Tuinstra, F., & Koenig, J. L. (1970). Raman spectrum of graphite. *The Journal of Chemical Physics*, 53, 1126–1130. <https://doi.org/10.1063/1.1674108>
- Vai, G. B., & Martini, I. P. (2001). Geomorphologic setting. In *Anatomy of an orogen: The Apennines and adjacent Mediterranean basins* (pp. 1–4). Springer. https://doi.org/10.1007/978-94-015-9829-3_1

- Verrucchi, C., & Minissale, A. (1995). Multivariate statistical comparison of Northern Apennines Paleozoic sequences: A case study for the formations of Monti Romani (Southern Tuscany-Northern Latium, Italy). *Applied Geochemistry*, *10*(5), 581–598. [https://doi.org/10.1016/0883-2927\(95\)00030-5](https://doi.org/10.1016/0883-2927(95)00030-5)
- Wilkins, R. W., Boudou, R., Sherwood, N., & Xiao, X. (2014). Thermal maturity evaluation from inertinites by Raman spectroscopy: The 'RaMM' technique. *International Journal of Coal Geology*, *128*, 143–152. <https://doi.org/10.1016/j.coal.2014.03.006>
- Wopenka, B., & Pasteris, J. D. (1993). Structural characterization of kerogens to granulite-facies graphite: Applicability of Raman microprobe spectroscopy. *American Mineralogist*, *78*, 533–557.
- Yui, T., Huang, E., & Xu, J. (1996). Raman spectrum of carbonaceous material: A possible metamorphic grade indicator for low-grade metamorphic rocks. *Journal of Metamorphic Geology*, *14*(2), 115–124. <https://doi.org/10.1046/j.1525-1314.1996.05792.x>